

Decaying post-flare loops system observed by SOHO/CDS and Yohkoh/SXT

M. Varady¹, A. Fludra², and P. Heinzel¹

¹ Astronomical Institute of the Academy of Sciences of the Czech Republic, 25165 Ondřejov, Czech Republic

² Space Science Department, Rutherford Appleton Laboratory, Chilton, OX11 0QX, UK

Received 20 September 1999 / Accepted 21 January 2000

Abstract. The results of an analysis of joint SOHO/CDS and Yohkoh/SXT observations of a decaying post-flare loops system with a rapid time evolution are presented. The loop system was a remnant of a small single loop flare (GOES class C2.9). Using the CDS raster taken in several EUV lines with different formation temperatures and a temperature sensitive line pair Fe XVI 360.8/Si XII 520.7 we confirmed the existence of the vertical stratification in the loop system according to the line formation temperature. The analysis of the SXT data showed a strong decay of the system with time. While the temperature of the hot part of the system ($T \simeq 2.5$ MK) decreased only slightly, the total emission measure dropped by more than a factor of four in approximately 10^3 s. This could be explained by a plasma outflow from the loops with velocity approximately 10 km/s. On the other hand, signs of rapid, probably radiative cooling can be identified in the images obtained from the CDS raster taken in cool lines of O V and O III. Using the density sensitive line pair of Fe XIV 334.2/353.8 and the integrated intensity of Fe XIV 334.2 line we determined the electron densities and emission measures across the top of the loop system. From the results of these measurements, taking all known uncertainties into account, we obtained that the geometrical filling factor at the top of the system in the regions with maximum electron density in the Fe XIV line lies in the interval from $\simeq 0.01$ to $\simeq 0.2$. A simple theoretical approximation of the energy balance in the post-flare plasma gives a total cooling time $\simeq 750$ s.

Key words: Sun: corona – Sun: flares – Sun: UV radiation – Sun: X-rays, gamma rays

1. Introduction

Systems of flare loops appear shortly after the onset of solar flares first in the soft X-ray and the EUV band and later on, H α loop prominences for events on the limb or typical dark loops on the disk usually appear (Bray et al. 1991). These loops are most conspicuous in the gradual phase of flares and can persist for many hours. This is also the reason why they are called in

literature ‘post-flare loops – PFL’ although their appearance during the impulsive phase is not unusual.

Sturrock (1968), Kopp & Pneumann (1976), Forbes & Malherbe (1986) and others proposed that PFL can result from a gradual reconnection of magnetic fields high in the solar corona which produces successively higher magnetic arches in the corona and at the same time, energy is released at the reconnection site (cusp) above the loop system. This energy is then transported downwards, along the magnetic field lines, either by thermal conduction or by beams of accelerated particles. As a consequence, the chromosphere and transition region are heated and a flow of evaporated hot plasma fills the corresponding magnetic loop system. A hot PFL is thus created. As the reconnection continues, this loop is separated from the energy input and starts to cool. In the meantime, a new hot PFL is originating above it.

PFL systems have been extensively observed particularly in H α and in soft X-rays, especially after the launch of Yohkoh with its Soft X-ray Telescope (SXT) (Tsuneta et al. 1991). H α images show plasma at temperatures around 10^4 K and provide very good spatial resolution useful for studies of the structural and dynamic properties of PFL (e.g. Wiik et al. 1996). From these observations it is also possible to determine the emission measure of cool plasma in the loop system (Schmieder et al. 1996). On the other hand, soft X-ray images, which lack the spatial resolution of H α images, show plasma with temperatures of the order of 10^6 – 10^7 K and they are useful for approximate temperature and emission measure analysis. The relation between cool (H α) and hot plasma in PFL systems was described in Schmieder et al. (1995).

Observations of PFL systems in EUV lines provide an excellent opportunity to study the behaviour of post-flare loop plasma at intermediate temperatures. EUV spectra also allow to apply efficient electron density, emission measure and temperature diagnostic methods (e.g. Mason & Monsignori Fossi 1994). Several studies of this kind have been published. Dere & Cook (1979) studied the time evolution of differential emission measure and electron density during the decay of a flare using data from Solrad 9 and Skylab. The spatial distribution of EUV emission and electron density was studied by Cheng (1980) using Skylab data. A displacement of loops visible in lines with high and low formation temperatures was found. Similar re-

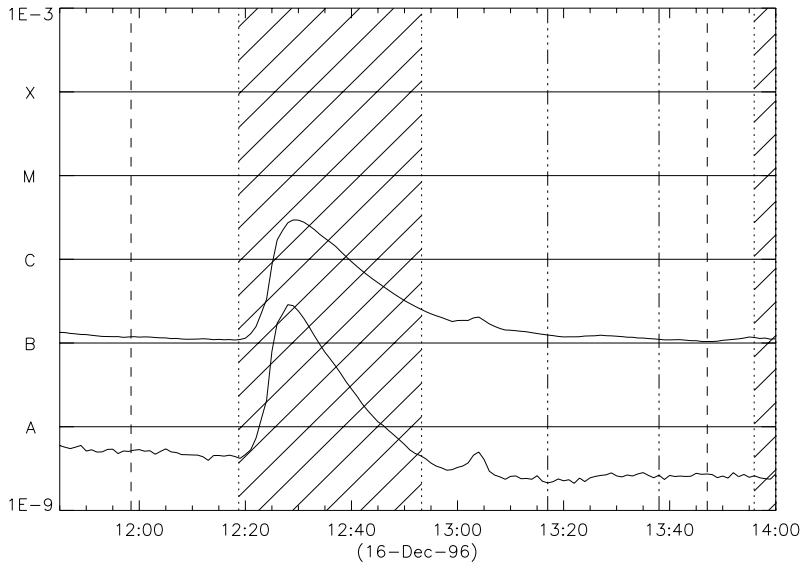


Fig. 1. GOES-9 X-ray fluxes and times of CDS and SXT observations. The hatched regions correspond to the times when the Yohkoh satellite was in the shadow of the Earth, the region between the two dashed lines corresponds to the time when the whole CDS raster was built and the region between the two dot-dash lines to the times when the loop system itself was scanned.

sults based on data from SMM and $H\alpha$ observations were also published by Švestka et al. (1987).

Using observations from SOHO Coronal Diagnostic Spectrometer (CDS) and Yohkoh SXT, we examine in this paper a decaying PFL system in its final phase when the loops are fading and becoming invisible. From SXT observations we derive the time evolution of the temperature and the emission measure in the hot part of the system during its decay. The CDS data was used to determine the vertical thermal structure of the examined loop system using the temperature sensitive line pair of Fe XVI at 360.8 Å and Si XII at 520.7 Å and its electron density from the density sensitive line pair of Fe XIV 334.2/353.8. From integrated intensities of several allowed lines with different formation temperatures the emission measures were calculated. From these measurements we estimated the geometrical filling factor at the top of the PFL system in Fe XIV lines. The values of the temperature and the electron density were then used to estimate the cooling time of the system from its initial temperature down to $\simeq 2 \times 10^4$ K.

2. Observations

The analysed PFL system was a remnant of a small flare (GOES class C2.9) which occurred on 16th December 1996 on the south-west limb of the Sun. GOES X-ray fluxes showed that the flare started at 12:20 UT, its maximum occurred at 12:29 UT and the GOES event finished at approximately 13:00 UT. There are no direct observations of the flare itself because during the flare Yohkoh was in the shadow of the Earth and the slit of CDS was high above the flare region. The data concerning the PFL system was taken only before and after the GOES event and its time distribution is presented on the background of GOES-9 X-ray fluxes in the Fig. 1.

2.1. CDS

The Coronal Diagnostic Spectrometer – CDS on board SOHO is fully described in Harrison et al. (1995) and Harrison & Fludra

(1995). The analysed raster was taken using the Normal Incidence Spectrometer (NIS) with the 2×240 arcsec slit oriented in the N–S direction.

The size of the raster analysed in this work is 243.8×240.2 arcsec, the spatial dimensions of one raster element are 2.032 arcsec in the E–W direction and 1.68 arcsec in the N–S direction. The exposure time of one spectrum was 45 s and the scanning started at 11:58:27 UT and finished at 13:47:05 UT (see also Fig. 1). The whole raster consists of 120 exposures and the total raster duration was 1h 48min 38s. This gives the CDS scanning speed $\simeq 54$ s per one N–S stripe. It is clear that when highly dynamic phenomena are observed, as for example PFL, a long scanning time can influence the shape of the observed structures and one has to be very careful when interpreting such observations. The observation was carried out in 16 spectral windows 20 pixels wide, in the spectral direction. Each window corresponds to spectral width approximately 1.33 Å for NIS I and 2.23 Å for NIS II. The spectral lines are usually in the middle of these windows. A list of the 14 spectral lines available and their approximate formation temperatures is given in Table 1. In addition to the 14 lines referred to in Table 1, there are two more spectral windows which are adjacent to the important density sensitive line pair of Fe XIV at 334.2 Å and 353.8 Å. These windows were used for determination of the scattered light level.

2.2. SXT

The Soft X-ray Telescope – SXT on board Yohkoh is described in detail in Tsuneta et al. (1991). The SXT is able to obtain time sequences of images in one of five filters with the time resolution better than one second. The pixel size of the CCD detector is 2.45 arcsec.

As we mentioned above, the Yohkoh satellite was in the shadow of the Earth during the flare (see Fig. 1), so that the only SXT images available were taken before and after the flare. In this analysis we used only the SXT data obtained after the flare.

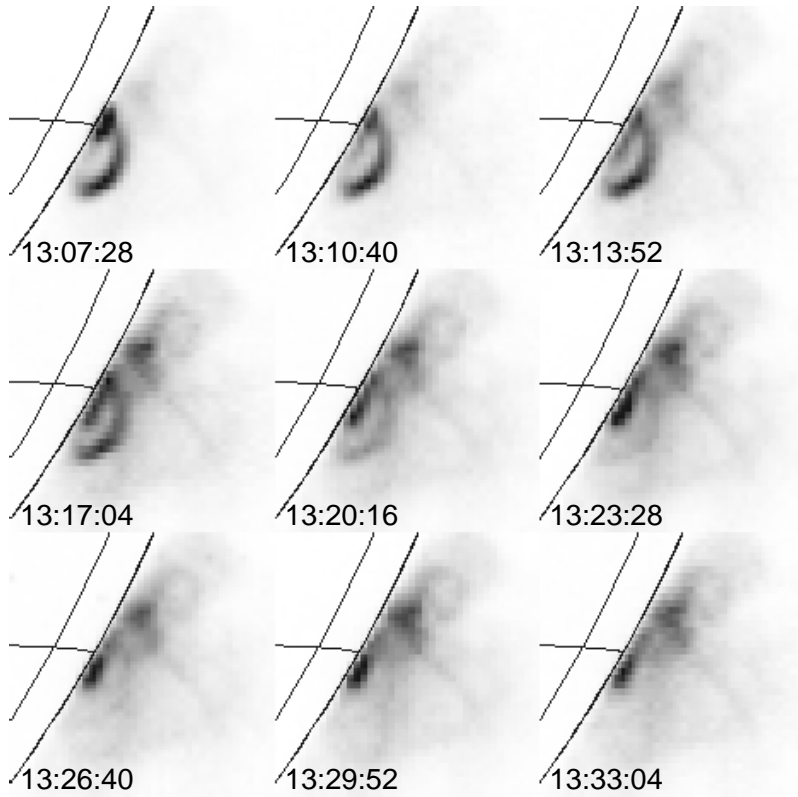


Fig. 2. A time sequence of Yohkoh SXT images taken in All filter showing the time evolution of the hot part of the PFL system. The times when the majority of these images was taken correspond to the times when the slit of CDS scanned the loop system (compare with Fig. 3).

Table 1. List of available lines and their formation temperatures. Asterisks indicate the density and crosses the temperature sensitive line pairs used in this analysis.

Ion	Wavelength Å	Temperature K
He I	584.33	2×10^4
O III	599.59	10^5
O V	629.73	2.5×10^5
Ca X	557.77	6×10^5
Mg IX	368.06	10^6
Mg X	624.94	1.1×10^6
Si X	347.40	1.3×10^6
Si X	356.04	1.3×10^6
Fe XII	364.47	1.6×10^6
Fe XIII	348.18	1.6×10^6
Si XII ⁺	520.67	1.8×10^6
Fe XIV*	334.17	1.8×10^6
Fe XIV*	353.83	1.8×10^6
Fe XVI ⁺	360.75	2.2×10^6

The first usable, not overexposed SXT image of the sequence of interest was taken at 13:07:28 UT and the last one a long time after the examined PFL system had disappeared. The time gap between two consecutive images was 64 s. The observational sequence was carried out in two filters. One image taken in All filter was followed by two images taken in AlMg filter. From the intensity ratio in these two filters the time evolution of the temperature and emission measure of the observed hot PFL plasma was determined.

3. Structure and time evolution of the PFL derived from SXT and CDS observations

The time evolution of the hot parts of the PFL system ($T \simeq 2.5$ MK), at approximately the same time when the slit of CDS scanned it, is very well visible in the images obtained by SXT (Fig. 2). A rapid evolution of the hot part of the loop system is seen in the first pictures of the sequence, while very little change is seen in the last images. The length of the loop determined from these pictures is approximately 2.5×10^9 cm. It is also apparent that the examined loop system is surrounded by a hot rare coronal plasma. An influence of this plasma has to be taken into account when the temperature, emission measure and electron density are determined. Apart from the PFL system and the rare coronal plasma around it, it is also possible to recognize some loops above PFL and two bright points; one above the northern footpoint of the loop and the second under it. These two bright points brighten when the PFL system is disappearing. In this analysis we discuss only the behaviour of the conspicuous loop-like structure visible in the first images of the sequence.

The CDS images of the PFL system, in eight selected lines which cover the temperature range from 2×10^4 K to 2.2 MK, are shown in Fig. 3. Here, in all lines roughly only one half of the loop system is clearly visible. Why this happens in the hot lines ($T > 1$ MK) is apparent from a comparison of the CDS images with the time sequence of images obtained by SXT (Fig. 2). The hot loops in the raster are visible until approximately 13:22 UT, which corresponds to the time when the hot loop observed by SXT starts to disappear as well. It will be shown in the next

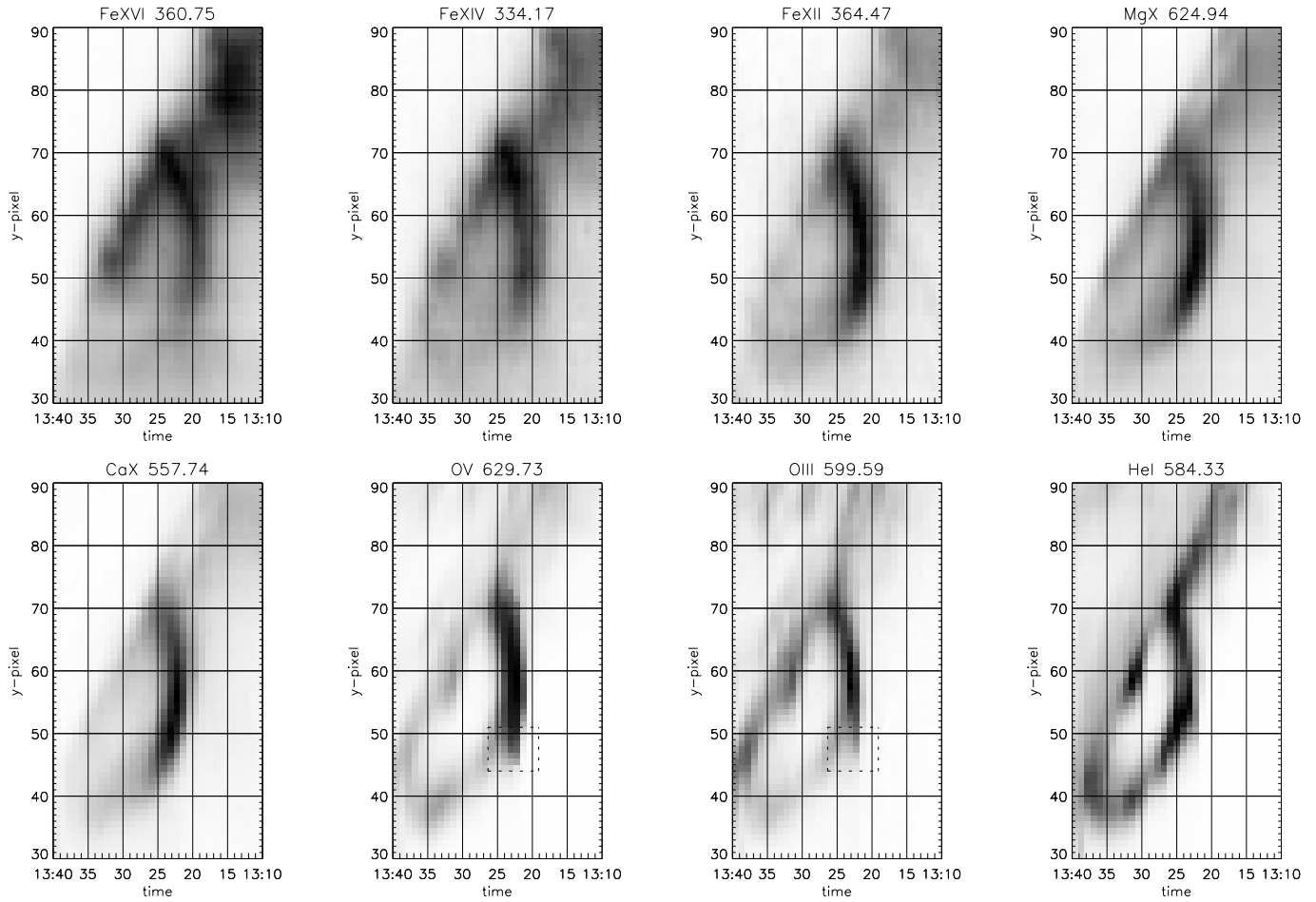


Fig. 3. Part of the CDS raster with the PFL system in eight chosen lines spanning the temperature range from 2×10^4 K to 2.2×10^6 K (image in negative). The times on the x -axes correspond to the positions of the CDS slit in the raster. The time goes from right to left because the CDS slit scans from W to E and is oriented in N–S direction.

section that this is mainly due to plasma depletion from the loop. In the cooler lines this could be due to the combined effect of plasma depletion and cooling.

It follows from the way the CDS rasters are built that the eight images with the loop-like structures in Fig. 3 are exactly cospacial. When the positions of the tops of the semi-loops taken in different lines are compared, it is apparent that those in the images which are taken in lines having higher formation temperature lay *above* those formed at lower temperatures. On the other hand, the structures visible in different lines are not spatially separated, but they are overlapping, which is demonstrated in Fig. 4. This temperature stratification with height can be either real, as it is supposed in theoretical models of PFL (Kopp & Pneumann 1976, Forbes & Malherbe 1986, etc.), or it could be mimicked by the combined effect of cooling and scanning the loop system with the CDS with a finite speed. The scanning across the loop tops in all available lines took approximately 5 min (see Fig. 3). In contrast, SXT measurements (Sect. 4) show that plasma cooling in the hot part of the system is very slow. Also the theoretical estimate of the PFL plasma cooling rate (Sect. 7) does not show any fast cooling in the temperature region above $\simeq 1$ MK which could explain the thermal

stratification of the loop system by the combined effect of cooling and scanning speed. We believe that at least in the lines with formation temperature above 1 MK we observe a real temperature stratification with height, as a ‘snapshot’ of the PFL system evolution.

When the shapes of the semi-loop structures visible in hot and cool lines are compared (Fig. 3), it is apparent that they are much smoother in the hot lines while in the cool lines there are some irregularities in their shapes (structures inside the dotted boxes). They are clearly not a part of the loop system, so they have to result from a combined effect of the PFL system time evolution and the finite scanning speed of CDS. We interpret these irregularities as a manifestation of a rapid cooling of PFL plasma visible in cool lines. If we admit that there is a real temperature stratification with height in the observed PFL system, then plasma with temperature a little higher than the formation temperature of the particular line is located above the bright loop tops seen in that line, and this hotter plasma is at that moment invisible in this line. But since the CDS slit scans the loop system with a finite speed approximately one step per minute (in Fig. 3 from right to left), the plasma with temperature just greater than the formation temperature of the particular line manages to cool

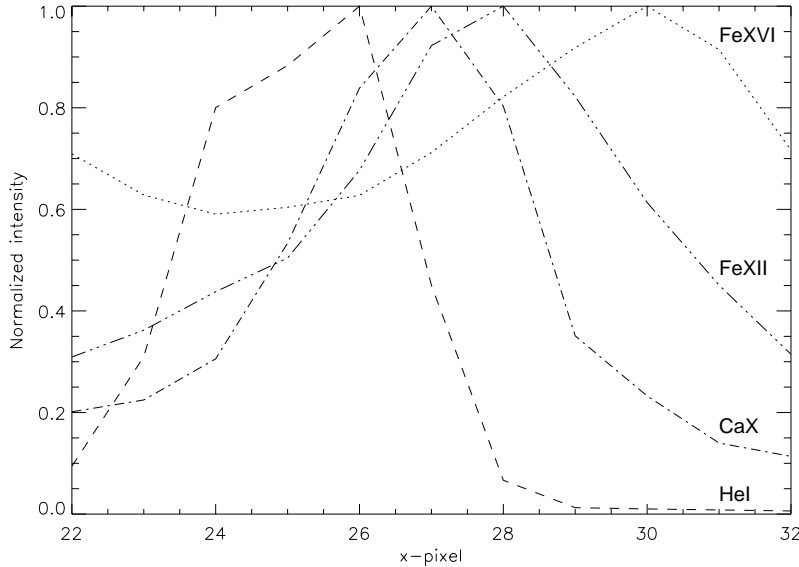


Fig. 4. Normalized intensity profiles of the CDS semi-loop structures taken in four selected lines He I, Ca X, Fe XII and Fe XVI. The intensity profiles are plotted along a horizontal line $y = 55$ in range from $x = 22$ (scanning time $\sim 13 : 27$) to $x = 32$ (scanning time $\sim 13 : 18$) (see also the raster plotted in the Fig. 6). To improve the S/N ratio we added to the corresponding $y = 55$ intensity intensities from two adjacent y pixels 54 and 56.

down and becomes visible as the irregularities in the loop-like structures. Because the time necessary for the completion of one N–S stripe exposure is approximately only one minute we can interpret these irregularities as a manifestation of very rapid, probably radiative plasma cooling visible in O V, O III and perhaps also He I lines. Since in the hot lines no similar features are seen, we believe that plasma visible here cools much more slowly compared to the CDS scanning speed.

Another prominent feature is the dependence of the sharpness (or diffusivity) of the PFL images on the formation temperature of the line which was used to take the image. From the CDS data available it follows that the images taken in hotter lines tend to be more diffused than the ones taken in cool lines, which are much sharper. On the other hand, for example, in the image taken in He I line (Fig. 3), the loop top where the CDS slit was parallel to the scanned structure is quite sharp but the part of the loop in the lower left corner, where the CDS slit was perpendicular to the scanned structure, is rather diffused. So we believe that this is probably caused by the combined effect of CDS scanning and different speed of plasma cooling in different lines, rather than by a real structural difference of hot and cool loops, although using this data we can not completely exclude the possibility of real structural difference of hot and cool loops.

4. Analysis of the SXT data

The SXT data and filter ratio method (Hara et al. 1992) were used to derive the time evolution of mean temperature and emission measure during the decay of the loop system. The intensity, in each filter (AlI, AlMg), was integrated from an area of 189 pixels which lay inside an intensity contour 39% above the background containing the whole loop (see Fig. 5). However, during the analysis we found out that the general behaviour of the mean plasma temperature and emission measure is almost independent of the chosen area of the loop system where the intensity was integrated from. A similar result was obtained by Schmieder et al. (1996).

The time evolution of the mean plasma temperature in the loop (upper graph in Fig. 5) looks rather complicated. At the beginning of the observational sequence, from 13:07:28 UT to 13:17:04 UT, a manifestation of slow plasma cooling from the initial temperature 2.8 MK down to 2.5 MK in approximately 600 s can be seen. Then the temperature behaves rather chaotic. We believe that this could be accounted for by the influence of hot rare coronal plasma surrounding the PFL system, the existence of which we mentioned in the previous section. When the emission measure of plasma inside the examined loop was much greater than the emission measure of other plasma along the line of sight, the manifestation of plasma properties in the examined loop prevailed over the manifestation of properties of surrounding plasma. But as the emission measure of plasma inside the loop was decreasing with time (see lower plot in Fig. 5), the measured quantities were more and more influenced by the properties and behaviour of other plasma lying along the line of sight. So we believe that plasma inside the PFL could continue cooling even after 13:17:04 UT because the values of the temperature later on are probably very strongly influenced by other hot coronal plasma along the line of sight (see Fig. 2).

The behaviour of the total emission measure along the line of sight averaged over the area of the whole loop $\langle EM_{tot} \rangle$, presented in the lower graph of Fig. 5, looks much simpler. It decreases very quickly (in approximately 960 s) from its original value $(9.2 \pm 0.3) \times 10^{28} \text{ cm}^{-5}$ at 13:07:28 UT to its final value $(2.2 \pm 0.2) \times 10^{28} \text{ cm}^{-5}$ at 13:23:28 UT. Because such a rapid decrease of $\langle EM_{tot} \rangle$ can be explained only by plasma depletion from the PFL (see also Fig. 2), we can expect a strong down-flow of hot plasma from the loop to its footpoints along the magnetic field lines. Later on, the behaviour of $\langle EM_{tot} \rangle$ becomes slightly chaotic again, which we believe can be accounted for by rare hot coronal plasma along the line of sight, with a mean emission measure $\langle EM_{cor} \rangle$, which does not belong to the PFL system. Because the emission measure is an additive quantity, the mean emission measure of plasma inside the loop system itself is

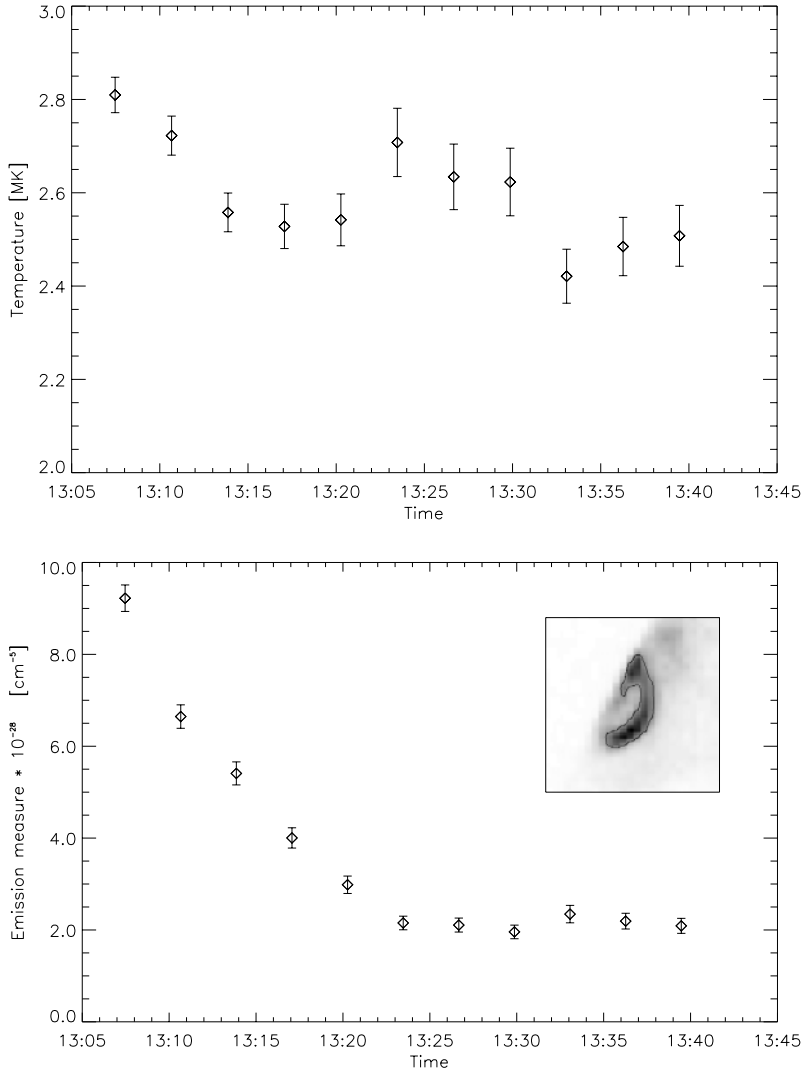


Fig. 5. The time evolution of mean temperature and emission measure for the whole loop (the region inside the intensity contour containing 189 pixels) obtained from the SXT observations using filter ratio method. The error bars include the decomposition and statistical errors. The systematic errors are not included.

$$\langle EM_{pfl} \rangle = \langle EM_{tot} \rangle - \langle EM_{cor} \rangle . \quad (1)$$

If the mean emission measure of plasma inside the loop system $\langle EM_{pfl} \rangle$ is known and if it is possible to estimate the size of the loop system D along the line of sight, a simple formula

$$\langle EM_{pfl} \rangle = \frac{1}{S_{pfl}} \int_{S_{pfl}} \int_0^D n_e^2 dl dS \approx \langle n_e^2 \rangle D \quad (2)$$

can be used to estimate the mean value of the second power of the electron density $\langle n_e^2 \rangle$ in the loop system. If we suppose that all the emitting plasma is deposited inside some filaments, which are not resolved by SXT and which have the same electron density, we can calculate the mean electron density in the volume occupied by the loop system: $\langle n_e \rangle = \sqrt{\langle n_e^2 \rangle}$. S_{pfl} is the area over which the intensity is integrated.

From the SXT images and CDS rasters (Figs. 2, 3) we determined the apparent diameter of the loop system in the plane perpendicular to the line of sight $D_{app} = (4.0 \pm 0.7) \times 10^8$ cm. If we assume that this apparent diameter obtained above equals D and $\langle EM_{pfl} \rangle = \langle EM_{tot} \rangle$, so that all the emitting plasma along the line of sight is concentrated in the loop system, the

maximum mean electron density is $(1.5 \pm 0.2) \times 10^{10}$ cm $^{-3}$ and the minimum density is $(7.0 \pm 1.0) \times 10^9$ cm $^{-3}$. On the other hand, if we suppose that $\langle EM_{cor} \rangle$ equals one half of the almost constant value of $\langle EM_{tot} \rangle$ at times from 13:23:28 UT to 13:39:28 UT, which is approximately $\langle EM_{tot} \rangle = (2.1 \pm 0.5) \times 10^{28}$ cm $^{-5}$ then the maximum mean electron density in the loop is $(1.4 \pm 0.2) \times 10^{10}$ cm $^{-3}$ and the minimum density is $(5.0 \pm 2.0) \times 10^9$ cm $^{-3}$, for the same value of D as in the previous case.

From the emission measure analysis we found that there has to be a plasma outflow from the examined loop system. Using the quantities obtained above and with the help of the continuity equation it is possible to estimate, though very roughly, the velocity of plasma outflow along the magnetic field at the base of the loop. If we suppose that the cross-sectional area along the loop is constant, we get for a velocity of a symmetrical plasma outflow to both footpoints ~ 10 km s $^{-1}$. If the plasma outflow is directed only to one footpoint of the loop system then the velocity would be approximately twice larger. This rather low velocity contrasts with much stronger flows ($v \sim 10^2$ km s $^{-1}$) observed in cool H α loops (Wiik et al. 1996). This could be

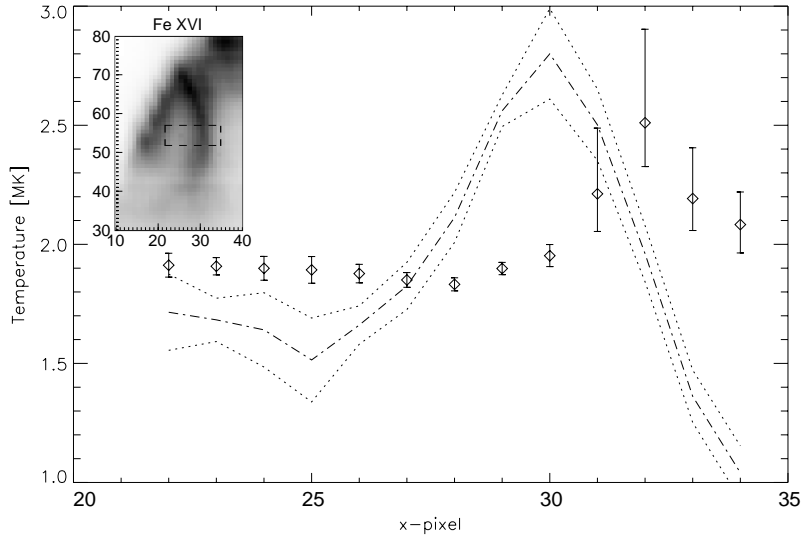


Fig. 6. The vertical thermal structure across the loop tops determined from the temperature sensitive ratio of Fe XVI 360.8 and Si XII 520.7 lines. The error bars correspond to 3σ probability of the fits. This graph is over-plotted by the normalized intensity profile of Fe XVI loop-like structure (dash-dot line) and by the errors in the intensities (dotted lines). In the upper left corner of the graph a part of the CDS raster was plotted. Its axis are in pixels which we refer all the measurements from CDS to. The dashed box is the region where the line intensities were measured.

explained by quite different pressure scale-heights in these two cases.

5. Analysis of the CDS data

5.1. Fitting the CDS spectral profiles

All results in this section were derived from integrated line intensities, taking their uncertainties into account. Because the way we obtained them was common in all following subsections, we will discuss it briefly here. We supposed that the spectra in individual spectral windows (covering the wavelength interval 1.33 \AA for NIS I and 2.33 \AA for NIS II) can be approximated by a sum of a constant b_0 representing the background (stray light) and L Gaussian components representing the individual spectral lines centered at wavelengths λ_k :

$$I_i = b_0 + \sum_{k=1}^L a_k \exp - \left(\frac{\lambda_i - \lambda_k}{\alpha c_k} \right)^2. \quad (3)$$

I_i is the intensity observed in the i -th spectral pixel at the wavelength λ_i , a_k is the amplitude, c_k is the FWHM of the k -th Gaussian and $\alpha \doteq 0.6$.

To obtain the best fit of parameters b_0 , a_k , λ_k and c_k , we used the least square method and minimized the function:

$$\sum_{i=1}^N \left[\frac{I_i}{\sigma_i} - \frac{1}{\sigma_i} \left(b_0 + \sum_{k=1}^L a_k \exp - \left(\frac{\lambda_i - \lambda_k}{\alpha c_k} \right)^2 \right) \right]^2, \quad (4)$$

where σ_i are the statistical errors in intensities collected in individual spectral pixels of the detector obtained from the photon statistics (Thompson 1997) and N is the number of spectral pixels. The searched integrated intensity of a given k -th line can be then easily calculated from fitted parameters a_k and c_k .

The statistical errors of the fitted parameters were calculated only for the parameters concerning the spectral line of interest which directly influence the searched integrated line intensity (i.e. a_s , c_s and b_0). These errors were obtained by a standard method described in detail in Press et al. (1989). Another source

of errors is the unknown accuracy in the calibration curves of CDS which can introduce a systematic error into the line intensities. Because this error is unknown, it could not be included, but when one is interested in a ratio of two line intensities with similar wavelengths lying on the same detector, these errors tend to cancel each other. This is the case of the density sensitive pair Fe XIV. On the other hand, for a ratio of two distant lines or two lines lying on different detectors it can be quite significant. This is the case of the temperature sensitive pair Fe XVI/Si XII.

5.2. CDS temperature diagnostics

To get information on the temperature distribution of hot plasma in the system across the loop tops we used the intensity ratio of lines Fe XVI at 360.8 \AA and Si XII at 520.7 \AA which is temperature sensitive in the interval from 1 MK to 3.2 MK. The theoretical intensity ratio is also dependent on the relative chemical abundance of iron to silicon which is not very well known (Meyer 1985) and which can also vary from flare to flare (Fludra & Schmelz 1995). Moreover, as we already mentioned above, the observed intensity ratio can be quite significantly influenced by the systematic error resulting from the uncertainty in the CDS calibration. These reasons prevented us from calibrating the temperature using only theoretical data and we had to use another method based on our knowledge of the temperature obtained from SXT data. Therefore, we supposed that the maximum temperature of plasma in the PFL system, measured using the line ratio, corresponds to the plasma temperature measured by SXT at the same time.

The ratios of Fe XVI and Si XII lines were determined in 13 pixels along the x axis from pixel numbers 22 – 34 (see Fig. 6). To improve the S/N ratio the signal was integrated from 6 pixels along the y axis from pixels 52 – 57. The error bars correspond to 3σ probability of the line fits and they do not contain any uncertainties in values of theoretically calculated emissivities. Their very variable length is given by the theoretical dependence of the temperature on the emissivities ratio. The emissivities were calculated using ADAS (Summers et al. 1996).

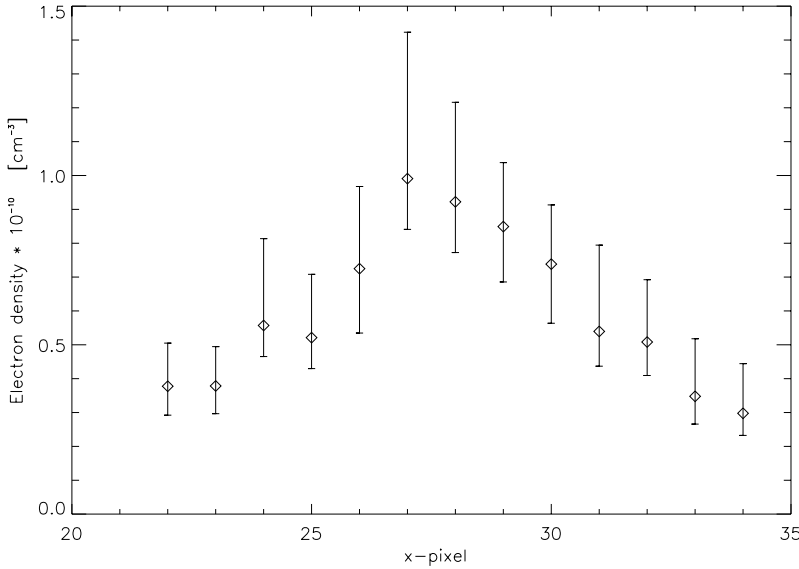


Fig. 7. The course of electron density determined from the ratio of intensities of the electron density sensitive line pair Fe XIV 334.2/353.8 across the top of the loop system. The error bars correspond to 3σ probability of the fits.

The results of this analysis are presented in Fig. 6, where the intensity profile of the Fe XVI loop was also plotted. It is clearly visible that the temperature increases with height and reaches its maximum above the Fe XVI loop. Plasma with lower density is probably located here. This distribution of temperature in the PFL system is in full agreement with the classical formation theory of PFL systems. The course of temperature under the Fe XVI loop reflects the temperature of rare hot coronal plasma surrounding the PFL system rather than the temperature of plasma located in the loops visible in lines having lower formation temperatures.

5.3. CDS electron density diagnostics

The CDS data was used to determine the electron density of the hot part of the PFL system, using the density sensitive line pair of Fe XIV 334.2/353.8 (Mason et al. 1997, Mason 1998). This line pair is electron density sensitive in range approximately from 10^9 cm^{-3} to 10^{11} cm^{-3} , where also the expected values of electron densities of PFL lie.

The disadvantage of this line pair is that when plasma with temperature greater than $\simeq 4 \text{ MK}$ is present in the analysed region, the Fe XIV line at 353.8 \AA is strongly blended with a very bright Ar XVI line. Fortunately the temperature analysis of the SXT data and also the comparison of observed spectra with the synthetic spectra calculated with CHIANTI (Dere et al. 1997, Mason 1998) showed that the plasma temperature in the analysed region is lower than $\simeq 3 \text{ MK}$, so that the blending is not prohibitive. The theoretical dependence of the electron density on the intensity ratio was calculated using CHIANTI.

The electron densities were determined in 13 different positions along the x axis across the loop top, in pixel numbers 22 – 34 (see the raster in Fig. 6). To improve the S/N ratio the intensity was integrated from 6 pixels along the y axis from pixels 52 – 57. To determine the level of scattered light we connected the spectral windows containing the given diagnostic lines with the adjacent spectral windows, and the minimum signal from

these two windows was taken as the background. The error bars correspond to 3σ probability of the line fits. No uncertainties are included in the theoretical dependence of electron density on the intensity ratio. The course of the electron density across the loop top is shown in Fig. 7. These values were used to estimate the geometrical filling factor in the top of the loop system.

5.4. CDS emission measure diagnostics

The integrated intensities of allowed lines with different formation temperatures were used to obtain the plasma emission measure using the method originally designed by Pottasch (1963). We assumed an isothermal plasma at temperature T , which corresponds to the maximum of the contribution function (emissivity) of the given line. Then the integrated intensity of the line can be approximated by a simple formula:

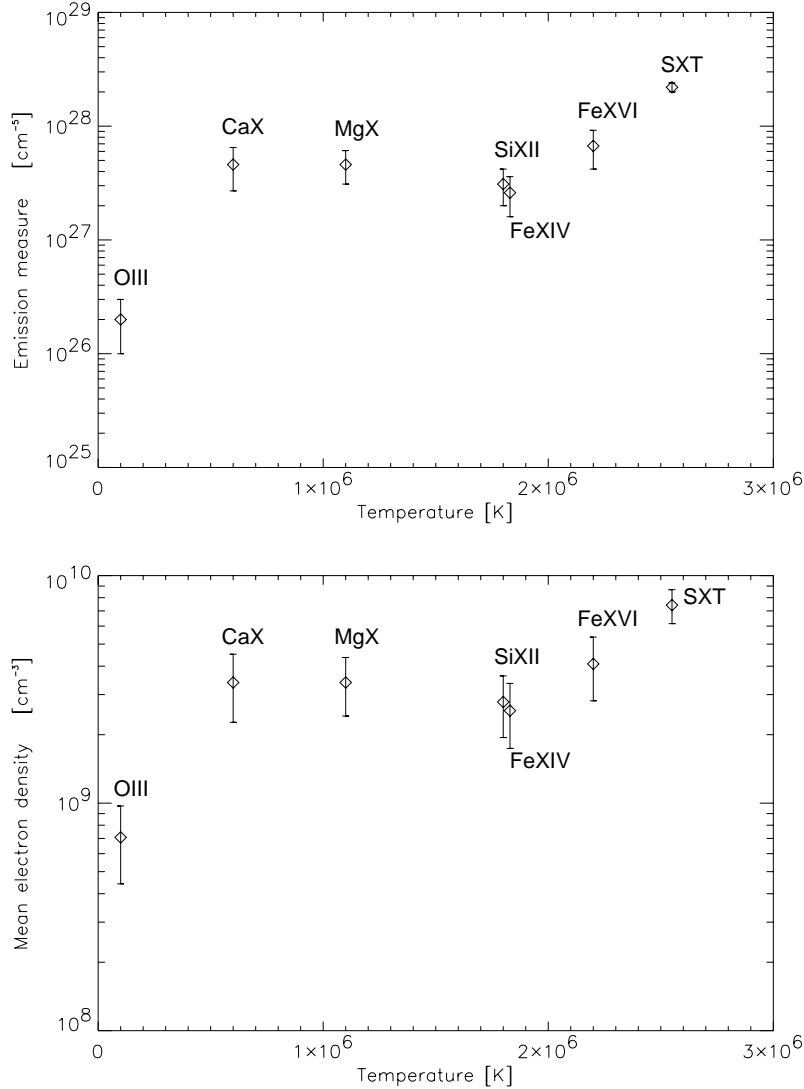
$$I = \frac{1}{4\pi} A G(T) EM, \quad (5)$$

where A is the elemental abundance relative to the hydrogen and I is the integrated intensity of the particular spectral line. The contribution functions $G(T)$ were calculated using ADAS (Summers et al. 1996) and the elemental abundances for a solar flare were taken from Fludra & Schmelz (1995). These abundances are subject to a 30% combined statistical and systematic uncertainty. The errors of integrated line intensities resulting from the photon statistics correspond to 3σ probability of the line fits.

The values of the emission measure were determined at the brightest regions at the tops of the loop-like structures visible in CDS raster in different spectral lines. These regions were one pixel broad in the x direction and the intensity was integrated from six pixels in the y direction. The results are summarized in Table 2 and the dependence of the emission measure on line formation temperature is shown in the upper plot in Fig. 8. Under the assumptions adopted in the Sect. 4 it is possible to determine the mean electron densities from these val-

Table 2. The results of the emission measure analysis.

Ion	Wavelength Å	Abundance	Emissivity $\times 10^{20}$ erg cm ³ s ⁻¹	x, y -coordinates pixels	Intensity erg cm ⁻² s ⁻¹ sr ⁻¹	$\langle EM \rangle \times 10^{-27}$ cm ⁻⁵
O III	599.59	2.5×10^{-4}	1.45	26, 54-59	63.8 ± 4.6	0.2 ± 0.1
Ca X	557.77	4.4×10^{-6}	5.57	26, 47-52	89.9 ± 9.7	4.6 ± 1.9
Mg X	624.94	4.0×10^{-5}	2.23	27, 50-55	323.8 ± 11.4	4.6 ± 1.5
Si XII	520.67	4.2×10^{-5}	1.64	28, 51-56	170.3 ± 7.9	3.1 ± 1.1
Fe XIV	334.17	4.8×10^{-5}	1.52	29, 52-57	153.4 ± 10.7	2.6 ± 1.0
Fe XVI	360.75	4.8×10^{-5}	2.19	30, 52-57	557.4 ± 37.8	6.7 ± 2.5

**Fig. 8.** The mean emission measures and electron densities obtained from allowed lines and SXT measurements versus the formation temperature of the lines. The emission measure is calculated for the brightest parts in the tops of corresponding loops (see Table 2).

ues of emission measure. We assumed that the size of the loop system along the line of sight corresponds to the apparent diameter of the loop system obtained from SXT and CDS images $D_{app} = (4.0 \pm 0.7) \times 10^8$ cm. The dependence of the electron density, obtained in this way, on the formation temperature is shown in the lower plot in Fig. 8. The mean electron densities for lines with formation temperatures from 2.2 MK (Fe XVI) to 0.6 MK (Ca X) remain almost constant with the temperature ($\simeq 3 \times 10^9$ cm⁻³). In contrast, the mean electron density cal-

culated from the emission measure derived from the intensity of O III is substantially smaller $\simeq 7 \times 10^8$ cm⁻³.

6. Plasma filling factor at the top of the PFL system

The results obtained from CDS electron density and emission measure analysis were used to estimate the geometrical filling factor of the examined PFL system in the Fe XIV line. If we assume that the plasma is isothermal and concentrated in fil-

aments with a typical electron density n_e , we can rewrite the formula for emission measure in this way:

$$EM = n_e^2 D_{real} = \langle n_e^2 \rangle D_{app} , \quad (6)$$

where

$$D_{real} = \int_{rad} dl . \quad (7)$$

In this integral we calculate the total thickness of the radiating elements along the line of sight. Using these quantities we can define the geometrical filling factor as

$$f \equiv \frac{D_{real}}{D_{app}} = \frac{\langle n_e^2 \rangle}{n_e^2} . \quad (8)$$

The density n_e in Eq. 8 has been derived from the density sensitive line ratio Fe XIV 334.2/353.8. This ratio measures the real electron density. The value of $\langle n_e^2 \rangle$ has been derived by dividing the emission measure EM , calculated from the allowed line intensity, by the apparent size of the system along the line of sight, D_{app} .

The quantities n_e^2 and $\langle n_e^2 \rangle$ are identical only in the case of homogeneous distribution of plasma along the line of sight. In this case the filling factor would be equal to one. If plasma is not distributed uniformly, the electron density obtained from line ratio is greater than the density obtained from the emission measure and the filling factor is less than one.

Using this method we determined the filling factor in pixels 26 – 30 (x axis) which correspond to the brightest parts of the Fe XIV loop-like structure. The uncertainties in n_e and $\langle n_e^2 \rangle$ obtained in previous subsections were used to calculate the uncertainty of the geometrical filling factor. The results are summarized in Table 3. From our measurements it follows that the geometrical filling factor at the top of the examined PFL system in the regions with maximum electron density in Fe XIV line (formation temperature $\simeq 1.8$ MK) lies in the interval from $\simeq 0.01$ to $\simeq 0.2$. The great range of its possible values reflects the realistic uncertainties in our knowledge of elemental abundance, integrated intensities and D_{app} .

The value of the geometrical filling factor in flare loops has an important consequence. The majority of flare loops observations have been made by Yohkoh/SXT. However, SXT can measure only the emission measure and not the electron density in observed regions. An approximation which assumes a homogeneous and isothermal plasma $n_e = \sqrt{EM/D}$ is often used to derive the electron density. This approximation does not take into account the possibility that the spatial plasma distribution can be filamentary. If we assume that the typical electron density in such filaments is approximately the same for all of them and the electron density outside the filaments is much smaller than inside, knowing the filling factor we can estimate the real electron density $n_e = \sqrt{EM/fD}$ of emitting elements with a much better accuracy.

7. Cooling of the PFL system

It is generally believed that the post-flare loop plasma cools mainly due to thermal conduction and radiation. To get a simple

Table 3. Geometrical filling factor across the top of the loop system determined using the Fe XIV 334.2 and 353.8 lines.

x -pixel	$n_e^2 \times 10^{-19}$ cm^{-6}	$\langle n_e^2 \rangle \times 10^{-18}$ cm^{-6}	f
26	$5.25^{+3.51}_{-2.76}$	4.3 ± 2.4	$0.08^{+0.10}_{-0.08}$
27	$9.81^{+8.57}_{-2.97}$	5.3 ± 2.8	$0.05^{+0.08}_{-0.04}$
28	$8.50^{+5.42}_{-2.76}$	6.1 ± 3.2	$0.07^{+0.08}_{-0.06}$
29	$7.21^{+3.21}_{-2.78}$	6.6 ± 3.5	$0.09^{+0.09}_{-0.08}$
30	$5.45^{+2.58}_{-2.58}$	5.9 ± 3.2	$0.11^{+0.11}_{-0.11}$

estimate of the time scale which a hot PFL with temperature of the order 10^6 K needs to reach temperature of the order 10^4 K, we used a simple formula of Švestka (1987) and we applied a correction to the temperature gradient introduced by Varady & Heinzel (1997). The formula was derived from the energy equation under the assumption of static ($n_e(t) = const$), fully ionized plasma. The first and the second term on the right hand side of the equation are approximations of conductive and radiative losses:

$$-3n_e k_B \frac{dT}{dt} = a \kappa_0 \frac{T^{7/2}}{L^2} + n_e^2 \chi T^\alpha . \quad (9)$$

In this equation $a = 0.4$ is the correction applied to the temperature gradient, k_B is the Boltzmann constant, L is the semi-length of the loop, $\kappa = 10^{-6}$ (in CGS units) is the thermal conductivity coefficient and χ and α fit the radiative losses. The latter were taken from Cargill (1994) and are based on the model of Cook et al. (1989):

$$\begin{aligned} \chi T^\alpha &= 2 \times 10^{-23} , & T > 10^{6.5} , \\ \chi T^\alpha &= 3.5 \times 10^{-7} T^{-2.5} , & 10^6 < T < 10^{6.5} , \\ \chi T^\alpha &= 3.5 \times 10^{-22} , & 10^5 < T < 10^6 , \\ \chi T^\alpha &= 1.1 \times 10^{-27} T^{1.1} , & T < 10^5 . \end{aligned} \quad (10)$$

Using the formula above and quantities obtained in previous sections we calculated the theoretical time dependence of plasma temperature in the PFL. The model was calculated for the initial temperature 2.8 MK, which was obtained from the SXT temperature analysis and a constant electron density 10^{10} cm^{-3} , which corresponds to the value obtained at the top of the loop system using the density sensitive line pair of Fe XIV. The theoretical time dependence of temperature in the loop is shown in Fig. 9. It follows from this model that the total cooling time required to achieve the temperature of the order 10^4 K is approximately 750 s. In fact the cooling time will probably be longer, because from the SXT emission measure analysis we have an evidence of a rapid decrease of emission measure in the loop system which reduces the radiative losses.

8. Discussions and conclusions

In this paper we used simultaneously taken CDS and SXT data to examine a decaying PFL system resulting from a small single

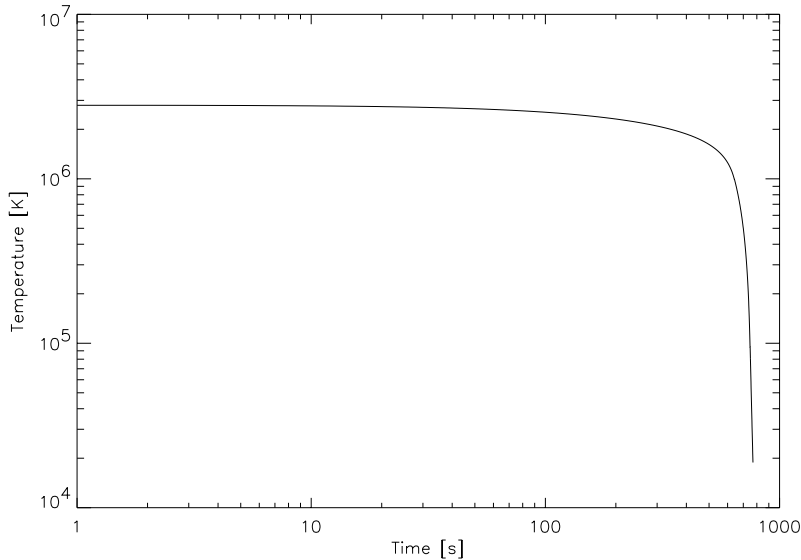


Fig. 9. Theoretical time dependence of the temperature of hot PFL, cooled conductively and radiatively from an initial temperature 2.8 MK. The electron density $n_e = 10^{10} \text{ cm}^{-3}$ in the loop is assumed to be constant with time.

loop flare GOES class C2.9. From the structural features contained in the CDS images taken in lines with different formation temperature we were able to confirm that plasma with higher temperature tends to lie over plasma with lower temperature, as it is expected by the PFL formation theory and which was earlier observed by Cheng (1980) and Švestka et al. (1987). Using the time evolution of temperature of hot plasma in the loop system derived from the SXT data and the theoretical estimate of the cooling time of the hot plasma in the PFL system we ruled out the possibility that the observed thermal distribution of plasma, emitting at different formation temperatures, could be mimicked by a combined effect of PFL plasma cooling and the CDS scanning speed. Another argument which supports the reality of the thermal stratification in the loop system is the existence of the irregularities observed in lines with formation temperatures under 0.5 MK which are protruding from the CDS loop-like structures. Providing the distribution of plasma temperature discussed above is real, these structures can be naturally explained as a result of a very fast plasma cooling, which can be expected at these temperatures. A similar result was obtained using the temperature sensitive line pair Fe XVI at 360.8 Å and Si XII at 520.7 Å. Using this line pair we found that the hottest plasma in the loop system is placed above the maximum intensity of the highest loop visible in Fe XVI line.

From the SXT emission measure and temperature analysis we obtained that the main role during the decay of the hot part of the loop system was played by a plasma outflow from the system. During approximately 10^3 s the mean emission measure in the loop decreased to roughly one fourth of its original value. The velocity of the plasma outflow from the loop system at the footpoints was estimated to be approximately 10 km s^{-1} , for a uniform cross-sectional area along the loop. The time evolution of temperature obtained from SXT data shows some signs of slow cooling at the beginning of the observational sequence. Later on, when the emission measure in the loop system substantially decreased, the temperatures are strongly influenced by the behaviour of the surrounding hot coronal plasma. When

we admit that the decrease of temperature observed at the beginning of the observational sequence represents a real plasma cooling and compare its speed to the speed of the emission measure loss, we can conclude that this part of the system decayed mainly due to plasma depletion from the system and the decrease of the temperature played a minor or perhaps a triggering role in the decay of the system. From the CDS data also follows that the plasma outflow from the PFL system, responsible for its decay, started in all lines at approximately the same moment.

To obtain the geometrical filling factor at the top of the PFL system in Fe XIV line ($\simeq 1.8 \text{ MK}$), we first determined the electron density and its uncertainty using the density sensitive line pair of Fe XIV. This method reflects the collisional rate in plasma and is not dependent on geometrical fine structural features in the system. Then we calculated emission measure of plasma in the system from the integrated intensities of an allowed line of Fe XIV at 334.2 Å (at the same locations where the electron densities using the density sensitive pair were measured). The emission measure was used to calculate the $\langle n_e^2 \rangle$ and its error. Because during the whole procedure of fitting and calculating of all the quantities necessary to determine the filling factor we took a great care to proper treatment of all errors which can influence the results, we obtained a great, but realistic uncertainty of the resulting filling factor. The results of our measurements are that the upper limit of the geometrical filling factor at the top of the loop system in Fe XIV line is $\simeq 0.2$ while the lower limit at least in regions of maximum electron density is $\simeq 0.01$. Of course, the filling factor can be different for loops with different temperatures. Unfortunately the CDS data available did not allow us to carry out a similar study in lines with different formation temperatures. The results show that if the electron density is estimated from for example a SXT emission measure without knowledge of the filling factor, the results can differ of factor from $\simeq 2$ to 10 from the real electron density in the observed region. This can strongly influence any theoretical interpretation of such observations.

Acknowledgements. MV acknowledges the financial support of ESA during his stay at the SOHO EOF where a substantial part of this study was carried out. MV is also indebted to P. C. Martens and A. J. C. Beliën for many fruitful discussions and to the whole CDS team for creating the excellent instrument. AF is supported by the United Kingdom PPARC. SOHO is a project of international cooperation between ESA and NASA. We thank B. Schmieder for useful comments. A part of this project was supported by a grant A3003902 of GA AV ČR.

References

- Bray R.J., Cram L.E., Durrant C.J., et al., 1991, Plasma loops in the solar corona. Cambridge Astrophysics Series 18, Cambridge University Press
- Cargill P.J., 1994, ApJ 422, 381
- Cheng C.-C., 1980, Sol. Phys. 65, 347
- Cook J.W., Cheng C.-C., Jacobs V.L., et al., 1989, ApJ 338, 1176
- Dere K.P., Cook J.W., 1979, ApJ 229, 772
- Dere K.P., Landi E., Mason H.E., et al., 1997, A&AS 125, 149
- Fludra A., Schmelz J.T., 1995, ApJ 447, 936
- Forbes T.G., Malherbe J.M., 1986, ApJ 302, L67
- Hara H., Tsuneta S., Lemen S., et al., 1992, PASJ 44, L135
- Harrison R.A., Sawyer E.C., et al., 1995, Sol. Phys. 162, 233
- Harrison R.A., Fludra A., 1995, The Coronal Diagnostic Spectrometer for the Solar and Heliospheric Observatory – Scientific Report, SC-CDS-RAL-SN-95-0001
- Kopp R.A., Pneumann G.W., 1976, Sol. Phys. 50, 85
- Mason H.E., Monsignori Fossi B.C., 1994, A&AR 6, 123
- Mason H.E., Young P.R., Pike C.D., et al., 1997, Sol. Phys. 170, No. 1, 143
- Mason H.E., 1998, In: Vial J.C., Bocchialini K., Boumier P. (eds.) Space Solar Physics. Lecture notes in physics 507, p. 143
- Meyer J.P., 1985, ApJS 57, 173
- Pottasch S.P., 1963, ApJ 137, 945
- Press W.H., Flannery B.P., Teukolsky S.A., et al., 1989, Numerical recipes. Cambridge University Press
- Schmieder B., Heinzel P., Wiik J.E., et al., 1995, Sol. Phys. 156, 337
- Schmieder B., Heinzel P., van Driel-Gesztelyi L., 1996, Sol. Phys. 165, 303
- Sturrock P.A., 1968, IAU Symp. 35, 471
- Summers H.P., Brooks D.H., Hammond T.J., et al., 1996, Atomic Data and Analysis Structure – User Manual, RAL-TR-96-017
- Švestka Z., 1987, Sol. Phys. 108, 411
- Švestka Z., Fontenla J.M., Machado M.E., et al., 1987, Sol. Phys. 108, 237
- Thompson W.T., 1997, CDS software note, No. 49
- Tsuneta S., Acton L., Ogawara Y., et al., 1991, Sol. Phys. 136, 37
- Varady M., Heinzel P., 1997, In: Wilson A. (ed.) Proc. of the Fifth SOHO Workshop, ESA SP-404, 7p. 05
- Wiik J.E., Schmieder B., Heinzel P., et al., 1996, Sol. Phys. 166, 89